

# The Bardeen-Cooper-Schrieffer supercurrent field-effect transistor

G. De Simoni,<sup>1</sup> F. Paolucci,<sup>1</sup> P. Solinas,<sup>2</sup> E. Strambini,<sup>1</sup> and F. Giazotto<sup>1,\*</sup>

<sup>1</sup>NEST, Istituto Nanoscienze-CNR and Scuola Normale Superiore, I-56127 Pisa, Italy

<sup>2</sup>SPIN-CNR, Via Dodecaneso 33, 16146 Genova, Italy

In their original formulation of superconductivity, the London brothers predicted more than eighty years ago [1] the exponential suppression of an *electrostatic* field inside a superconductor over the so-called London penetration depth,  $\lambda_L$  [2, 3], in analogy to the Meissner-Ochsenfeld effect [4].  $\lambda_L$  ranges from a few tens to a few hundreds of nanometers for Bardeen-Cooper-Schrieffer (BCS) superconductors [4, 5]. A superconducting body smaller than  $\lambda_L$  is thereby expected to be entirely penetrated and, in principle, affected by electrostatic fields. Yet, the lack of any proof [6] has led to the general belief that superconductors behave like normal metals [5] expelling electrostatic fields over the sub-atomic Thomas-Fermi screening length ( $\sim 0.5\text{\AA}$ ) [7]. Despite a few experiments suggesting hints of penetration [8–11], no clue has been provided so far on the possibility to manipulate conventional superconductors via field effect. Here we report the evidence of electrostatic field penetration leading to full field-effect control of the supercurrent in *all-metallic* transistors made of a BCS superconductor. At low temperature, our titanium field-effect transistors (FETs) show a monotonic decay of the critical current under increasing electrostatic field up to total quenching for gate voltage values as large as  $\pm 40\text{V}$ . The field effect persists up to  $\sim 85\%$  of the critical temperature ( $\sim 0.41\text{K}$ ), and in the presence of sizable magnetic fields. A similar behavior, though less pronounced, was observed in aluminum FETs. An *ad hoc* phenomenological theory based on the Ginzburg-Landau formalism [12] accounts for our observations and proves the truthfulness of London's original hypothesis. Besides shedding light on a fundamental milestone in physics, our results represent a groundbreaking asset for the realization of an *all-metallic* superconducting field-effect electronics. Moreover, they are pivotal for boosting the implementation of leading-edge quantum information architectures based on Josephson FETs [13, 14].

In BCS theory [4, 5], conventional superconductivity is described as the co-existence of a ground state, namely, the condensate formed by Cooper pairs, and quasiparticle excitations living for energies above the superconducting energy gap,  $\Delta$ . These so-called Bogolubov quasiparticles, or ‘bogolons’, are created by breaking of Cooper pairs, for instance, by thermal fluctuations, and consist of a coherent superposition of electron- and hole-like excitations with opposite spin [4, 15]. Owing to their mixed nature, bogolons have energy-dependent charge [4, 15–17] which can be *zero*, i.e., bogolons are neutral, at the gap edge  $\Delta$  [4, 15, 16]. The reduced bogolons charge should thus weakly screen electrostatic fields inside a superconductor, in stark contrast to what free electrons do in normal

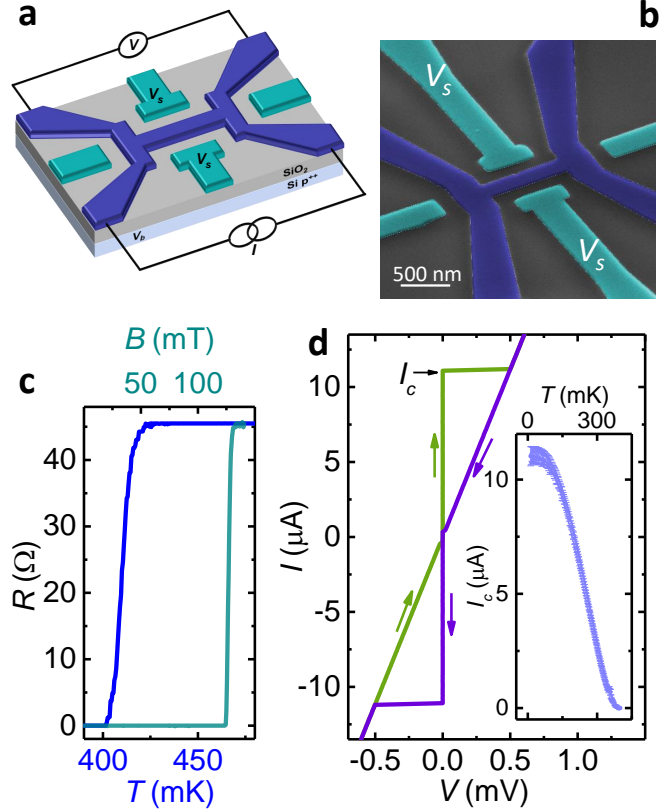


FIG. 1. **The BCS supercurrent field-effect transistor: pre-characterization.** **a**, Schematic of the *all-metallic* supercurrent FET. Back and side gate voltage denoted with  $V_b$  and  $V_s$ , respectively, are used to control the amplitude of the Ti wire critical supercurrent.  $V_b$  is applied to the  $p^{++}$  Si substrate. In four-probe measurements, an electric current  $I$  is fed into the superconducting wire whereas the voltage drop  $V$  is simultaneously recorded as a function of the applied gate voltage. **b**, Pseudo-color scanning electron micrograph of a representative Ti supercurrent FET. The wire length is 900 nm while the width is 200 nm, and the thickness is 30 nm. The transistor core is shown in blue whereas the Ti side gates are colored in cyan. **c**, Resistance  $R$  vs temperature  $T$  (blue line, bottom horizontal axis), and  $R$  vs perpendicular-to-plane magnetic field  $B$  at 5 mK (light blue line, top horizontal axis) characteristics of the supercurrent FET. The normal-state resistance of the device is  $R_N \sim 45\Omega$ . **d**, Field-effect transistor current ( $I$ ) vs voltage ( $V$ ) characteristic measured in a four-probe configuration at 5 mK.  $I_c \simeq 11\mu\text{A}$  denotes the wire switching critical current. The inset shows the full temperature evolution of  $I_c$ , and its quenching at the critical temperature ( $T_c \sim 410\text{mK}$ ). The error bars represent the standard deviation of the critical current  $I_c$  calculated over 50 measurements.

metals [7], and should permit the interaction with the Cooper condensate, as envisioned by the early London theory [1]. It

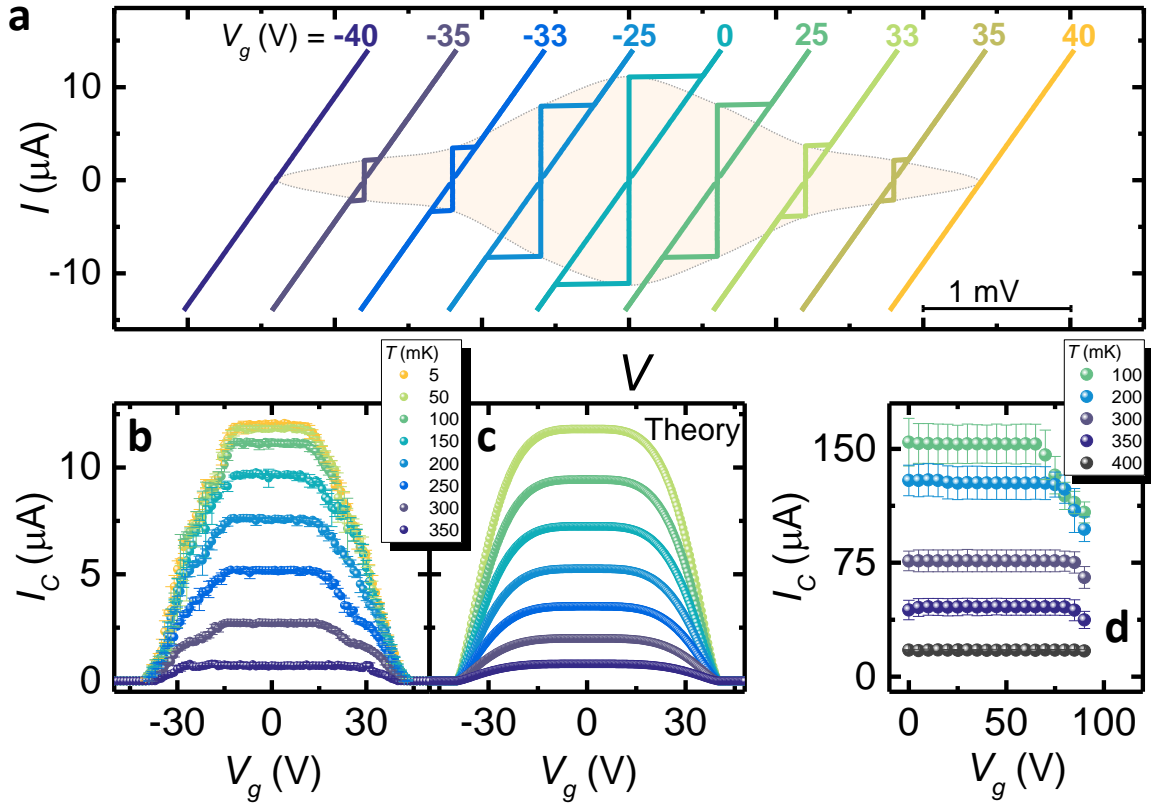


FIG. 2. **Electrostatic-field dependence of the supercurrent FET.** **a**, Current-voltage ( $I-V$ ) characteristics of a Ti supercurrent FET measured at 5 mK for several values of the applied gate voltage ( $V_g \equiv V_b = V_s$ ). Hatched area is a guide to the eye emphasizing the monotonic suppression of the critical current  $I_c$  down to zero by increasing  $V_g$ . When the supercurrent vanishes, the  $I(V)$  characteristics coincide with that in the normal state, independently of the value of the applied gate voltage. The curves are horizontally offset for clarity. **b**, Behavior of the critical current  $I_c$  vs  $V_g$  measured at different bath temperatures  $T$ . Note the full suppression of  $I_c$  occurring for  $|V_g| \gtrsim 40$  V. This threshold voltage turns out to be almost independent of bath temperature. **c**, Phenomenological critical current  $I_c$  vs  $V_g$  characteristics calculated with an *ad hoc* model based on Ginzburg-Landau formalism for the same values of bath temperature as in panel b. We stress the agreement with the experimental data provided by the model, both for the monotonic decay of the  $I_c(V_g)$  characteristics and for the temperature independence of the threshold voltage ( $V_g^c$ ) over which full suppression of  $I_c$  occurs. **d**,  $I_c$  vs  $V_g$  characteristics measured at different bath temperatures  $T$  of a  $4\mu\text{m} \times 4\mu\text{m}$  FET showing electrostatic field-tuning of the critical current occurring in a two-dimensional (with respect to  $\lambda_L$ ) superconducting structure. In this case, the maximum achieved  $I_c$  relative reduction is around  $\sim 30\%$  at 100 mK. Here, the electrostatic field was applied only through the back gate ( $V_g \equiv V_b$ ). A critical temperature  $T_c \simeq 470$  mK, and a perpendicular-to-plane magnetic critical field  $B_c \simeq 115$  mT are the main characteristic parameters of the Ti film realizing this 2D FET. The error bars in panel b and d represent the standard deviation of the critical current  $I_c$  calculated over 50 and 20 measurements, respectively.

is the aim of this Letter to address this fundamental question in physics whilst providing through an extraordinarily simple approach answers to this puzzling, and so far unsolved paradigm.

A generic scheme of our all-metallic supercurrent FETs is displayed in Fig. 1a. The transistors have been fabricated by electron-beam lithography and evaporation of titanium (Ti) on top of an  $p^{++}$ -doped Si substrate covered by a 300-nm-thick  $\text{SiO}_2$  insulating layer (see Methods Summary for further details). Back and side gate voltages, denoted by  $V_b$  and  $V_s$ , respectively, are used to generate the electrostatic field that controls the supercurrent flow in the wire. Figure 1b shows a pseudo-color scanning electron micrograph of a typical device. The Ti FET consists of a wire of length  $l = 900$  nm, width  $w = 200$  nm, and thickness  $t = 30$  nm. Similar transis-

tors with length up to a  $3\mu\text{m}$  have shown the same behavior. From the critical temperature  $T_c \simeq 410$  mK [see Fig. 1c showing the wire resistance ( $R$ ) vs temperature ( $T$ ) characteristic (blue line)] we determined the zero-temperature BCS energy gap,  $\Delta_0 = 1.764k_B T_c \simeq 62\mu\text{eV}$ , where  $k_B$  is the Boltzmann constant. With this parameter, and from the low-temperature normal-state resistance of the wire,  $R_N \simeq 45\Omega$ , we deduced the London penetration depth,  $\lambda_L = \sqrt{\hbar R_N w t / (\pi \mu_0 l \Delta_0)} \simeq 900$  nm where  $\mu_0$  is the vacuum magnetic permeability. Since  $w, t \ll \lambda_L$ , the superconductor can be uniformly penetrated by external magnetic fields and, in principle, by electrostatic fields applied perpendicularly to the wire [1]. Figure 1c displays the wire  $R$  vs perpendicular-to-plane  $B$  characteristic at 5 mK (light blue line) revealing a magnetic critical field as large as  $\sim 127$  mT.

Below  $T_c$ , dissipationless charge transport occurs in the transistor through Cooper pairs supercurrent. The wire current-voltage ( $I - V$ ) characteristics recorded at 5mK is shown in the main panel of Fig. 1d. In particular, a switching critical current with amplitude  $I_c \simeq 11\mu\text{A}$  is observed displaying the usual hysteretic behavior which stems from heating induced in the wire while switching from the resistive to the dissipationless regime [18]. The monotonic decay of  $I_c$  as a function of temperature, and its full quenching at  $T_c$  is shown in the inset of Fig. 1d.

Investigation of field effect in our system is performed by current biasing the superconducting wire, and by measuring the critical current vs gate voltage ( $V_g$ ) applied simultaneously to the back and side gates so that  $V_b = V_s \equiv V_g$  (see Fig. 1a). This gate bias configuration maximized the impact of the electric field on  $I_c$ . Figure 2a shows the transistor  $I - V$  characteristics measured at 5mK for increasing values of  $V_g$ . Remarkably, the critical current is monotonically reduced by increasing  $V_g$ , and is fully suppressed at a critical voltage  $|V_g^c| \simeq 40\text{V}$ . Moreover, the effect is almost symmetric in the polarity of  $V_g$ . At a first glance, this  $I_c$  behavior might resemble the one achieved in semiconductor-based Josephson FETs [13, 14, 19–23] though our transistors are fully *metallic* so that the electric field does not affect the  $I - V$  characteristic when the wire switches into the normal state. Moreover, the supercurrent FET is fully *bipolar*. Analogous behavior was also observed in aluminum FETs with a maximum achieved  $I_c$  reduction of  $\sim 35\%$  (see SI). We speculate that the impressive  $I_c$  suppression and quenching originates from field-effect-induced localization and squeezing of the superconducting pairing potential in the wire, and is the hallmark of the penetration of a static electric field inside a BCS superconductor smaller than  $\lambda_L$ .

The full temperature dependence of field effect in the transistor is shown in Fig. 2b that displays the  $I_c$  vs  $V_g$  characteristics for several bath temperatures. Increasing  $T$  the critical current plateau widens, which might be ascribed to enhanced screening from the large number of thermally excited bogolons. At the same time, the critical voltage  $V_g^c$  determining full suppression of  $I_c$  is almost temperature independent. Notably, field effect persists up to about  $\sim 85\%$  of  $T_c$ , i.e.,  $\sim 350\text{mK}$ , and proves the extraordinary penetration of the electric field occurring even at elevated temperatures.

A simplified description of the  $I_c$  behavior in our system can be obtained through an *ad hoc* phenomenological model developed within the Ginzburg-Landau formalism [12] (see SI for details). According to our model, the wire critical current can be written as

$$I_c(T, V_g) = I_c^0 \left(1 - \frac{T}{T_c}\right)^{3/2} \left[1 - \left(\frac{V_g}{V_g^c}\right)^4\right]^{3/2}, \quad (1)$$

where  $I_c^0$  is the zero-temperature, zero-gate voltage wire critical current. Figure 2c shows the  $I_c$  vs  $V_g$  characteristics calculated from Eq. (1) for the same temperatures as in panel

b. In the calculations we used the values for  $T_c$  and  $V_g^c$  determined from the experiment. Although idealized, this theory is a useful tool to grasp the essential features of our FETs such as the  $I_c$  plateau widening by increasing the temperature, and the  $T$ -independent behavior of the critical voltage  $V_g^c$ .

Figure 2d displays the  $I_c$  vs  $V_g$  characteristics measured at different temperatures of a square-shaped transistor consisting of a  $4 - \mu\text{m}$ -long side, and the same film thickness. This structure was conceived to prove the field effect also on a two-dimensional (2D) superconducting region with lateral dimensions largely exceeding  $\lambda_L$ . The curves reveal a similar field-effect-induced  $I_c$  suppression though with reduced intensity with respect to wires, as here only the back gate  $V_b \equiv V_g$  was applied. Nevertheless, this remarkable result proves that the spatial scale relevant for penetration is the one parallel to the applied electric field, in full analogy to the Meissner-Ochsenfeld effect. Therefore, even in 2D thin films ( $t \ll \lambda_L$ ),  $I_c$  can be deeply affected by a perpendicular electrostatic field.

We now discuss the joined impact of both electric and magnetic fields on the supercurrent in the wire. The perpendicular-to-plane magnetic field dependence of the FET critical current at 5mK and  $V_g = 0$  is shown in Fig. 3a. Here we note the magnetic field-induced drop of  $I_c$ , and its full suppression at  $\sim 127\text{mT}$ . Furthermore, the fine structure visible on the non-monotonic  $I_c(B)$  characteristic can be ascribed to the penetration of Abrikosov vortices in the Ti film upon increasing  $B$  [24]. The full  $I_c$  dependence on  $V_g$  for several magnetic fields at 5mK is summarized in Fig. 3b. Similarly to temperature, by increasing  $B$  leads to a widening of the  $I_c$  plateau, which could stem from enhanced screening produced both by the rising amount of quasiparticles at higher magnetic field and by free electrons within the normal core of the vortices. The threshold voltage  $V_g^c$  turns out to be only very weakly dependent on  $B$ . We stress how considerable is the impact of the electric field effect even in the presence of magnetic fields approaching the critical one. Yet, our model still provides a successful description of the experimental data (see SI for details), as shown in Fig. 3c.

Finally, quantification of the spatial penetration of the electric field in the superconductor at 5mK and  $B = 0$  is provided in Fig. 3d where the  $I_c$  suppression parameter ( $\mathcal{S}$ ), defined as  $\mathcal{S} = 100 \times [I_c(V_{si} = 0) - I_c(V_{si} = 90\text{V})]/I_c(V_{si} = 0)$  (with  $i = 1, 2$ , see the inset of panel d displaying a representative comb-like device) whilst keeping the back gate voltage fixed at  $V_b = 45\text{V}$ , is shown. Differing from Figs. 2a,b and 3b, a higher  $V_{si} = 90\text{V}$  gate voltage value was set to provide sizeable supercurrent suppression via a single side gate.  $\mathcal{S}$  was determined for each wire composing an on-purpose designed comb-like Ti FET, and it is plotted vs the wire distance ( $x$ ) of the center of each wire from the lateral edges of the comb. A clear and substantial fading of field effect-induced suppression of  $I_c$  is observed by increasing the distance. Dashed line is an exponential decay fit to the data from which we extract an attenuation length  $\lambda \simeq 770 \pm 150\text{nm}$ , in good agreement with the penetration depth  $\lambda_L \sim 900\text{nm}$  previously estimated in our Ti films. Moreover, measurements of  $\lambda$  at different bath tem-

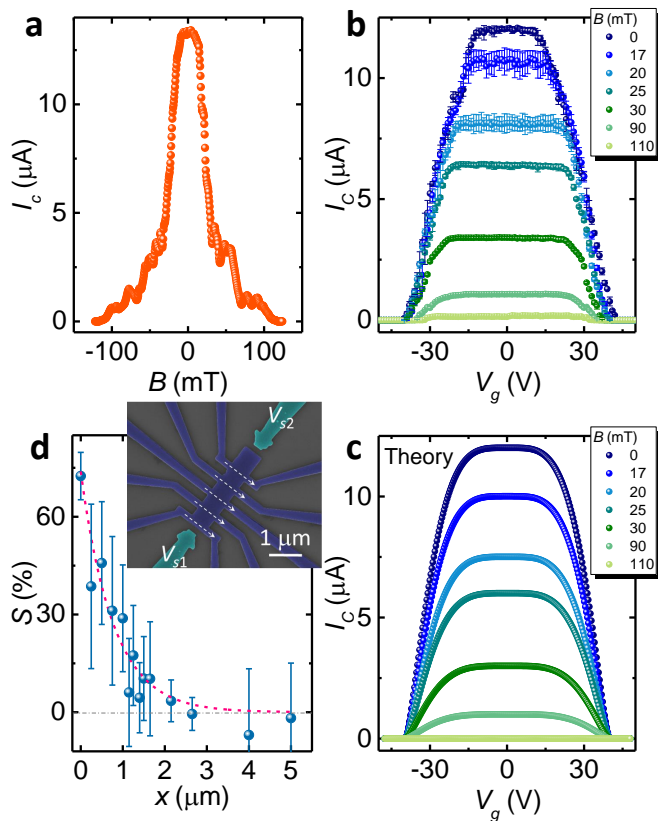


**FIG. 3. Magnetic-field dependence of the FET, and spatial penetration of the electric field.** **a**, Typical pattern of the critical current  $I_c$  vs perpendicular-to-plane magnetic field  $B$  measured at 5 mK for  $V_g = 0$ . **b**, Behavior of  $I_c$  vs  $V_g$  measured at 5 mK for several values of the perpendicular magnetic field. **c**, Theoretical critical current  $I_c$  vs  $V_g$  characteristics calculated at 5 mK for the same values of magnetic field as in panel **b**. **d**, The inset shows a pseudo-color scanning electron micrograph of a typical Ti comb-like FET used to investigate the spatial penetration of the electrostatic field in the superconductor. White dashed arrows indicate the direction of the critical current measured in each wire composing the comb. The on-purpose asymmetry of device geometry allows to use the same wire for two  $I_c$  measurements at different distances from the side gates. The main panel displays the critical current suppression parameter ( $S$ ) vs distance  $x$  measured at 5 mK for  $B = 0$ . The suppression parameter represents the relative  $I_c$  reduction for  $V_g = 90$  V with respect to zero applied side gate voltage, so that  $S = 0$  indicates the absence of field-effect induced suppression of the critical current.  $x$  represents the average distance of the center of each wire from the lateral edges of the comb. The critical current of each wire is recorded by polarizing one side gate at the time (i.e.,  $V_{s1} \neq 0$  or  $V_{s2} \neq 0$ ) while keeping the back gate voltage fixed at  $V_b = 45$  V. The plot summarizes all  $S$  values measured in two different comb-like FETs having an average distance of 500 nm and 1  $\mu$ m between the superconducting wires. Dashed line is an exponential damping fit to the data [ $S(x) = S_0 \exp(-x/\lambda)$ ] with a decay length  $\lambda \simeq 770 \pm 150$  nm. The error bars in panel **b** and **d** represent the standard deviation of the critical current  $I_c$  and  $S$ , respectively, calculated over 50 measurements.

peratures reveal that the electrostatic field penetration depth is almost constant within the experimental error up to  $\sim 80\%$  of

$T_c$ , then rapidly decreasing and vanishing by approaching the critical temperature (see SI for details).

Our results on supercurrent FETs confirm the original prediction of London brothers of more than eighty years ago [1], namely, the substantial penetration of a conventional BCS superconductor by a static electric field. Besides offering solution to a long-standing and fundamental issue in physics, the discovered effect represents an outstanding tool to envision a revolution in terms of novel-concept superconducting field-effect devices ranging from tunable Josephson weak-links [13, 14] or interferometers [25] to Coulombic [26] and coherent caloritronic structures [27] as well as single-photon detectors [28], which would exploit field effect to enhance their functionalities. Given the general nature of our findings which is intrinsic to any BCS superconductor, there is a large flexibility for the optimization of this method both from the technological and material point of view. On the one hand, improved gating schemes exploiting thinner insulators could easily enable the reduction of gate voltage amplitudes by more than one order of magnitude. On the other hand, alternative superconductors such as very thin NbN films ( $t < 10$  nm) with  $T_c$  larger than 10 K, and penetration depth approaching 500 nm [29, 30] could be ideal candidates for the implementation of an all-metallic high-speed superconducting field-effect electronics.

## METHODS SUMMARY

### Fabrication details and experimental set-up

The supercurrent FETs were fabricated with electron-beam lithography, and evaporation of metal through a resist mask onto a  $\text{SiO}_2/p^{++}\text{-Si}$  commercial wafer. The deposition of Ti was performed at room temperature in an ultra-high vacuum electron-beam evaporator with a base pressure of  $\sim 10^{-10}$  Torr at a deposition rate of  $\simeq 11 - 13 \text{ \AA/s}$ .

The magneto-electric characterization of the FETs was performed in a filtered  $\text{He}^3\text{-He}^4$  dry dilution refrigerator at different bath temperatures down to 5 mK using a standard 4-wire technique. The current vs voltage characteristics of the FETs were obtained by applying a low-noise biasing current, with voltage across the superconducting nanowire being measured by a room-temperature battery-powered differential preamplifier. Gate biasing was provided by a low-noise voltage source whereas a low-frequency lock-in technique was used either for resistance vs temperature or resistance vs magnetic field measurements.

## ACKNOWLEDGEMENTS

The authors wish to thank J. E. Hirsch for fruitful comments, and for having drawn the attention to relevant questions on fundamental issues related to BCS superconductivity so far considered well established. J. S. Moodera and A.



Shanenko are acknowledged for useful discussions. The European Research Council under the European Unions Seventh Framework Program (FP7/2007-2013)/ERC Grant agreement No. 615187-COMANCHE, and MIUR-FIRB2013 Project Coca (Grant No. RBFR1379UX) are acknowledged for partial financial support. The work of G.D.S. and F.P. was funded by Tuscany Region under the FARFAS 2014 project SCIADRO. The work of E.S. was partially funded by the Marie Curie Individual Fellowship MSCAIFEF-ST No. 660532-SuperMag. P.S. has received funding from the European Union FP7/2007-2013 under REA Grant agreement No. 630925-COHEAT.

#### AUTHOR CONTRIBUTIONS

G.D.S. and F.P. fabricated the samples, and performed the measurements with the help of E. S. G.D.S. and F.P. analyzed the experimental data with input from E.S. and F.G. P.S. developed the theoretical model with input from F.G., and performed the numerical calculations. F.G. conceived the experiment on field effect, and wrote the manuscript with input from all authors. All authors discussed the results and their implications equally at all stages.

#### COMPETING FINANCIAL INTERESTS

The authors declare no competing financial interests.

---

\* [francesco.giazotto@sns.it](mailto:francesco.giazotto@sns.it)

- [1] London, F. & London, H. The Electromagnetic Equations of the Supraconductor. *Proc. Roy. Soc. A* **149**, 71-88 (1935).
- [2] Hirsch, J. E., Charge expulsion and electric field in superconductors. *Phys. Rev. B* **68**, 184502 (2003).
- [3] Hirsch, J. E., Electrodynamics of superconductors. *Phys. Rev. B* **69**, 214515 (2004).
- [4] Tinkham, M. *Introduction to Superconductivity* (McGraw-Hill, 1996).
- [5] Bardeen, J., Cooper, L. N. & Schrieffer, J. R. Theory of Superconductivity. *Phys. Rev.* **108**, 1175-1204 (1957).
- [6] London, H. An Experimental Examination of the Electrostatic Behaviour of Supraconductors. *Proc. Roy. Soc. A* **155**, 102-110 (1936).
- [7] Ashcroft, N. W. & Mermin, N. D. *Solid State Physics* (Thomson Learning, Toronto, 1976).
- [8] Tao, R., Xu, X., Lan, Y. C. & Shiroyanagi, Y. Electric-field induced low temperature superconducting granular balls. *Physica C* **377**, 357-361 (2002).
- [9] Tao, R., Xu, X. & Amr, E. MgB<sub>2</sub> superconducting particles in a strong electric field. *Physica C* **398**, 78-84 (2003).
- [10] Hirsch, J. E., Explanation of the Tao Effect: Theory for the Spherical Aggregation of Superconducting Microparticles in an Electric Field. *Phys. Rev. Lett.* **94**, 187001 (2005).
- [11] Moro, R., Xu, X., Yin, S. & de Heer, W. A. Ferroelectricity in Free Niobium Clusters. *Science* **23**, 1265 (2003).
- [12] Ginzburg, V. L. & Landau, L. D. On the theory of superconductivity. *Zh. Eksp. Teor. Fiz.* **20**, 35 (1950).
- [13] Larsen, T. W., Petersson, K. D., Kuemmeth, F., Jespersen, T. S., Krogstrup, P., Nygård, J. & Marcus, C. M. Semiconductor-Nanowire-Based Superconducting Qubit. *Phys. Rev. Lett.* **115**, 127001 (2015).
- [14] Casparis, L., Larsen, T.W., Olsen, M.S., Kuemmeth, F., Krogstrup, P., Nygård, J., Petersson, K.D., & Marcus, C.M. Gate-mon Benchmarking and Two-Qubit Operations. *Phys. Rev. Lett.* **116**, 150505 (2016).
- [15] de Gennes, P. G. *Superconductivity of Metals and Alloys*, Advanced Books Classics (Westview Press, 1999).
- [16] Blonder, G. E., Tinkham, M. & Klapwijk, T. M. Transition from metallic to tunneling regime in superconducting microconstrictions: Excess current, charge imbalance, and supercurrent conversion. *Phys. Rev. B* **25**, 4515-4532 (1982).
- [17] Ronen, Y., Cohen, Y., Kang, J.-H., Haim, A., Rieder M.-T., Heiblum M., Mahalu, D. & Shtrikman, H. Charge of a quasiparticle in a superconductor. *PNAS* **113**, 1743-1748 (2016).
- [18] Courtois, H., Meschke, M., Peltonen, J. T. & Pekola, J. P. Origin of Hysteresis in a Proximity Josephson Junction. *Phys. Rev. Lett.* **101**, 067002 (2008).
- [19] Takayanagi, H. & Kawakami, T. Superconducting Proximity Effect in the Native Inversion Layer on InAs. *Phys. Rev. Lett.* **54**, 2449-2452 (1985).
- [20] Kleinsasser, A. W., Jackson, T. N., McInturff, D., Rammo, F. & Pettit, G. D. Superconducting InGaAs junction field-effect transistors with Nb electrodes. *Appl. Phys. Lett.* **55**, 1909-1911 (1989).
- [21] Akazaki, T., Takayanagi, H., Nitta, J. & Enoki, T. A Josephson field effect transistor using an InAs-inserted-channel In<sub>0.52</sub>Al<sub>0.53</sub>As/In<sub>0.53</sub>Ga<sub>0.47</sub>As inverted modulation-doped structure. *Appl. Phys. Lett.* **68**, 418-420 (1996).
- [22] Doh, Y.-J., van Dam, J. A., Roest, A. L., Bakkers, E. P. A. M., Kouwenhoven, L. P. & De Franceschi, S. Tunable Supercurrent Through Semiconductor Nanowires. *Science* **309**, 272-275 (2005).
- [23] Xiang, J., Vidan, A., Tinkham, M., Westervelt, R. M. & Lieber, C. M. Ge/Si mesoscopic Josephson junctions. *Nat. Nanotechnol.* **1**, 208-213 (2006).
- [24] Morgan-Wall, T., Leith, B., Hartman, N., Rahman, A. & Marčević, N. Measurement of Critical Currents of Superconducting Aluminum Nanowires in External Magnetic Fields: Evidence for a Weber Blockade. *Phys. Rev. Lett.* **114**, 077002 (2015).
- [25] Clarke, J. & Braginski, A. I. (eds) *The SQUID Handbook* (Wiley-VCH, 2004).
- [26] Grabert, H. & Devoret, M. (eds) *Single Charge Tunneling: Coulomb Blockade Phenomena in Nanostructures* Ch. 1 (Springer, 1992).
- [27] Fornieri, A. & Giazotto, F. Towards phase-coherent caloritronics in superconducting circuits. *Nat. Nanotechnol.* **xx**, xxx (2017).
- [28] Gol'tsman, G. N., Okunev, O., Chulkova, G., Semenov, A., Smirnov, K., Voronov, B. & Dzardanov, A. Picosecond superconducting single-photon optical detector. *Appl. Phys. Lett.* **79**, 705-707 (2001).
- [29] Kamlapure, A., Mondal, M., Chand, M., Mishra, A., Jesudasan, J., Bagwe, V., Benfatto, L., Tripathi, V. & Raychaudhuri, P. Measurement of magnetic penetration depth and superconducting energy gap in very thin epitaxial NbN films. *Appl. Phys. Lett.* **96**, 072509 (2010).
- [30] Shapoval, T., Stopfel, H., Haindl, S., Engelmann, J., Inosov, D. S., Holzapfel, B., Neu, V. & Schultz, L. Quantitative assessment of pinning forces and magnetic penetration depth in NbN thin films from complementary magnetic force microscopy and transport measurements. *Phys. Rev. B* **83**, 214517 (2011).

## SUPPLEMENTARY INFORMATION

### Temperature dependence of electrostatic field penetration depth $\lambda$ in Ti FETs

We have also measured the suppression parameter  $\mathcal{S}$  as a function of distance  $x$  at different bath temperatures in a comb-like Ti FET having an average distance of 500nm between the superconducting wires. For each temperature, an exponential decay fit to the  $\mathcal{S}(x)$  data allowed to extract the corresponding attenuation length  $\lambda$ . The result of this procedure is shown in Fig. 4 which displays the measured  $\lambda(T)$  curve. Specifically, we note the substantial temperature *independence* of the electrostatic field penetration depth up to  $\sim 330$ mK, which corresponds to about 80% of the critical temperature of the Ti film composing the comb-like transistor ( $T_c \sim 430$ mK). A further increase of the temperature above 330mK yields a rapid decay of  $\lambda$ , up to its full quenching around 375mK. We speculate that the observed drastic suppression of the penetration length occurring at high temperature might be induced by enhanced screening of the electrostatic field stemming from the large number of bogolons existing near the critical temperature. This makes the behavior of the superconducting wire almost similar to that of a normal metal by approaching  $T_c$ .

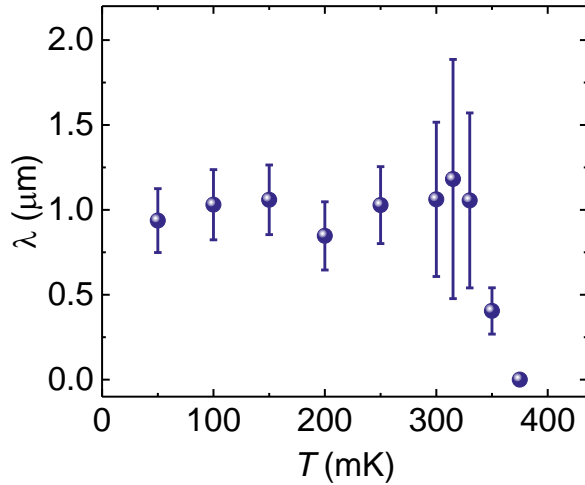


FIG. 4. **Temperature dependence of the electrostatic field penetration depth  $\lambda$ .** Behavior of  $\lambda$  vs  $T$  measured in a Ti comb-like FET having an average distance of 500nm between the superconducting wires. A critical temperature  $T_c \simeq 430$ mK characterizes the Ti film realizing this transistor.  $\lambda$  is almost temperature independent up to  $\sim 330$ mK, and then rapidly decays to zero by approaching  $T_c$ .

### Aluminum (Al) supercurrent FETs

Analogous results for field effect-induced suppression of the critical current were observed in FETs made of aluminum (Al). In particular, the Al FETs consist of a wire of length  $l = 800$ nm, width  $w = 30$ nm, and thickness  $t = 11$ nm. From

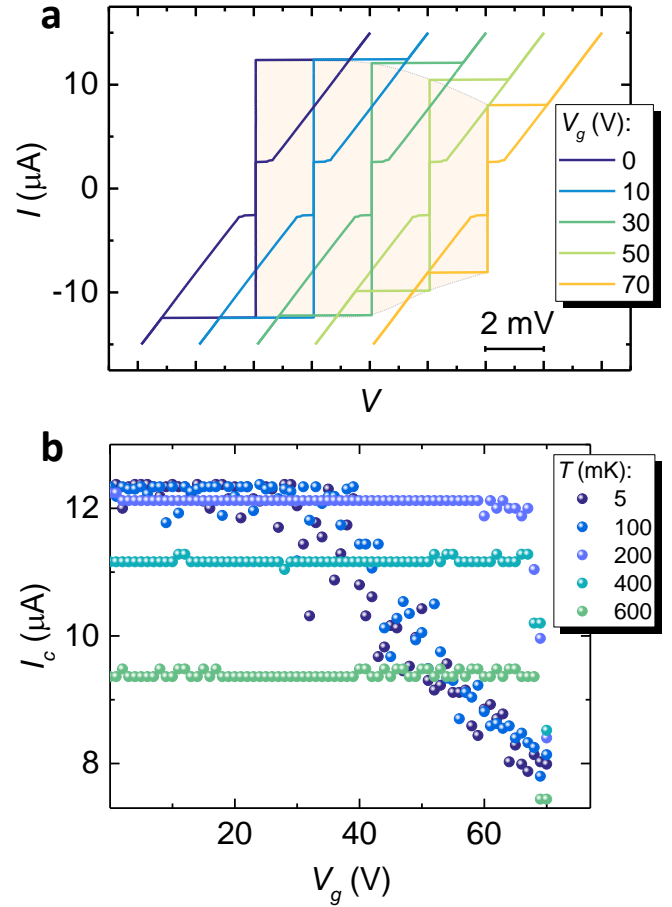


FIG. 5. **Electrostatic field dependence of the Al supercurrent FET characteristics.** **a**, Current-voltage ( $I - V$ ) characteristics of an Al supercurrent FET measured at 5 mK for several values of the applied gate voltage ( $V_g \equiv V_b = V_s$ ). Hatched area is a guide to the eye emphasizing the monotonic suppression of the critical current  $I_c$  by increasing  $V_g$ . Similarly to Ti superconducting FETs, when the supercurrent vanishes the Al FET  $I(V)$  characteristics coincide with that in the normal state, independently of the applied voltage. The curves are horizontally offset for clarity. **b**, Behavior of the transistor critical current  $I_c$  vs  $V_g$  measured at different bath temperatures  $T$ . Note the monotonic suppression of  $I_c$  occurring for  $V_g \gtrsim 35$ V at temperatures below 100mK. This threshold voltage for supercurrent suppression largely increases at higher bath temperature.

the normal-state resistance of the wire,  $R_N \simeq 320\Omega$ , and critical temperature,  $T_c \simeq 1.5$ K, we deduce the London penetration length  $\lambda_L \simeq 310$ nm, and the superconducting coherence length  $\xi_0 \simeq 63$ nm assuming  $\mathcal{N}_F = 2.15 \times 10^{47} \text{J}^{-1} \text{m}^{-3}$  for the density of states at the Fermi energy of our Al films. For these wires holds as well the condition  $w, t \ll \lambda_L$  so that substantial modulation of the critical current occurs under the application of an external static electric field.

Figure 5a shows the wire current vs voltage ( $I - V$ ) characteristics recorded at 5mK for several values of the applied gate voltage with  $V_b = V_s \equiv V_g$ . In the present case of Al transistors, the switching critical current at zero gate voltage obtains values as high as  $I_c \simeq 12.3\mu\text{A}$ , which is reduced down to

$\sim 8\mu\text{A}$  for  $V_g = 70\text{V}$  corresponding to a relative suppression of the order of  $\sim 35\%$ . Similarly to Ti supercurrent FETs, the current-voltage characteristics show a clear hysteretic behavior but with a larger retrapping current. The electric field does not affect the  $I - V$  characteristics when the wire switches to the normal state. Furthermore, differently from  $I_c$ , the retrapping current is unaffected by  $V_g$ . We note that for the Al FETs it was impossible to totally quench the critical current within the explored values of  $V_g$ .

The full temperature dependence of field effect in the wire is displayed in Fig. 5b where the  $I_c$  vs  $V_g$  characteristics are shown for a few selected bath temperatures. In particular, a monotonic suppression of  $I_c$  occurs for  $V_g \gtrsim 35\text{V}$  at temperatures below 100mK. At higher temperature, the threshold voltage for  $I_c$  suppression moves towards larger values while at the same time the critical current reduction turns out to be somewhat limited. Field effect in these Al transistors persists up to  $\sim 600\text{mK}$ , i.e., around 40% of critical temperature. The reduced impact of electric field on  $I_c$  might be ascribed to the much smaller London penetration depth  $\lambda_L$  characterizing these Al FETs in comparison to that obtained in Ti films.

### Phenomenological theory for field effect-induced suppression of $I_c$

In the absence of magnetic field, the superconducting free energy  $F$  reads [1–3]:

$$F = F_n + \alpha(T)|\psi|^2 + \frac{\beta}{2}|\psi|^4 + \frac{\hbar^2}{2m}|\nabla\psi|^2 + \frac{\mathcal{E}_{tot}^2}{8\pi}. \quad (2)$$

Following Ginzburg-Landau theory,  $\alpha = \alpha_0(T/T_c - 1)$  and  $\beta$  parameters describe the transition from superconducting to normal state. The superconducting state is obtained for  $\alpha < 0$  and order parameter minimum is found for  $\psi = \psi_0 = -\alpha/\beta$  [1, 2]. The term  $F_n$  represents the free energy in the normal state, whereas the last term is the energy associated to the total electric field  $\mathcal{E}_{tot}$ . In our case, the interesting term is  $\nabla\psi$  that describes the deformation of  $\psi$  and, indirectly, it includes the effects of the electric field.

We consider a wire with length  $d_x$  and lateral dimensions  $d_y$  and  $d_z$  (with  $d_x \gg d_y, d_z$ ) and, accordingly, we set the coordinate axis (see Fig. 6). The current flows along the  $x$  direction and the extremes of the wire are at  $y = \pm d_y/2$  and  $z = \pm d_z/2$ . The electric fields are applied along the  $y$  and  $z$  directions.

We write the order parameters as  $\psi = \psi_x \psi_y \psi_z$ . Along the current flowing direction  $\psi$  is uniform, i.e.,  $\psi_x = \psi_0 f$  where  $f$  is a space-independent parameter keeping into account the modulation of  $\psi$ . Our working assumption is that the presence of the electric field *squeezes* the order parameter  $\psi$  along  $y$  and  $z$  directions. To simplify the treatment, the squeezing is described by Gaussian functions centered in  $y = 0$  and  $z = 0$  and with standard deviation  $\sigma_y$  and  $\sigma_z$ . Accordingly, we have

$$\psi = \psi_0 f \left( \frac{e^{-\frac{y^2}{2\sigma_y^2}}}{\sqrt{2\pi} \sigma_y/d_y} \right)^{\frac{1}{2}} \left( \frac{e^{-\frac{z^2}{2\sigma_z^2}}}{\sqrt{2\pi} \sigma_z/d_z} \right)^{\frac{1}{2}}. \quad (3)$$

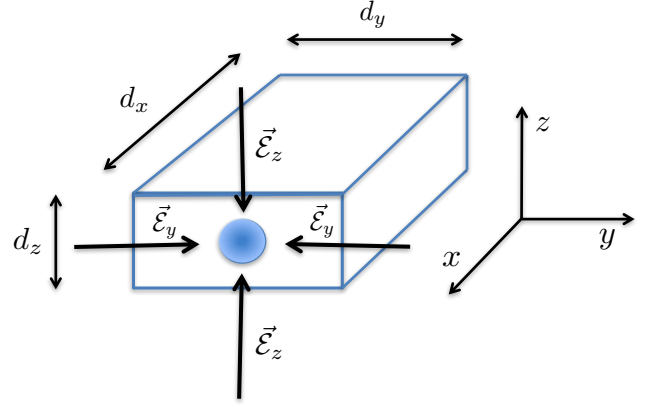


FIG. 6. **Effect of electric fields on a superconducting wire.** A superconducting wire of length  $d_x$ ,  $d_y$  and  $d_z$  is subject to electric fields  $\vec{\mathcal{E}}_y$  and  $\vec{\mathcal{E}}_z$ . The electric fields produce a squeezing of the Ginzburg-Landau order parameter (shown as a blue circle) along the field directions. The current flows along the  $x$  direction.

An increase of the electric field  $\mathcal{E}_i$  along the  $i$ -th direction leads to a squeezing of the order parameter along the same direction and, thus, to a decrease of  $\sigma_i$ . To describe this effect we assume that  $\sigma_i = \mathcal{V}/\mathcal{E}_i$  where  $\mathcal{V}$  has the dimension of a voltage.

Keeping track of the spatial modulation of  $\psi$ , the free energy (2) becomes

$$F = F_n + \alpha\psi^2 + \frac{\beta}{2}\psi^4 + \frac{\hbar^2}{8m} \left( \frac{y^2}{\sigma_y^4} + \frac{z^2}{\sigma_z^4} \right) \psi^2 + \frac{\mathcal{E}_{tot}^2}{8\pi}. \quad (4)$$

By minimizing the latter with respect to  $\psi$ , we arrive at the equation  $\alpha + \beta\psi^2 + \frac{\hbar^2}{8m} \left( \frac{y^2}{\sigma_y^4} + \frac{z^2}{\sigma_z^4} \right) = 0$  and, using the relations  $\alpha = -|\alpha|$  and  $\psi_0 = |\alpha|/\beta$ , we obtain

$$-|\alpha|(1 - f^2\psi_y^2\psi_z^2) = \frac{\hbar^2}{8m} \left( \frac{y^2}{\sigma_y^4} + \frac{z^2}{\sigma_z^4} \right). \quad (5)$$

We take the average over  $y$  and  $z$  directions, i.e.,  $1/d_y \int_{-d_y/2}^{d_y/2} dy$  and  $1/d_z \int_{-d_z/2}^{d_z/2} dz$ . For  $\sigma_i \ll d_i$ , we have that  $1/d_y \int_{-d_y/2}^{d_y/2} \psi_y^2 dy \approx 1/d_y \int_{-\infty}^{\infty} \psi_y^2 dy = 1$  and  $1/d_y \int_{-d_y/2}^{d_y/2} y^2 dy = d_y^2/12$  and analogously for the  $z$  coordinate.

For a symmetric wire, and equal applied electric fields we have  $d_y = d_z = d$ ,  $\mathcal{E}_y = \mathcal{E}_z = \mathcal{E}$ ,  $\sigma_y = \sigma_z = \sigma$  and  $f^2 = 1 - \frac{\hbar^2}{48m|\alpha|} \frac{d^2}{\sigma^4}$  that can be written as

$$f^2 = 1 - \frac{1}{\bar{\alpha}(T)} \left( \frac{\mathcal{E}}{\mathcal{E}_c} \right)^4 \quad (6)$$

where we have used  $\sigma = \mathcal{V}/\mathcal{E}$  and defined  $\bar{\alpha}(T) = |\alpha(T)|/\alpha_0 = (T_c - T)/T_c$  and  $\alpha_0 \equiv \alpha(T = 0)$  that has the dimension of an energy.

In equation (6) we have introduced an electric critical field  $\mathcal{E}_c = [48m\alpha_0 V^4 / (\hbar^2 d^2)]^{1/4}$ . Since  $0 \leq \psi \leq \psi_0$ , we have that

$0 \leq f \leq 1$ . Equation (6) tells us that if  $\mathcal{E} \geq \bar{\alpha}^{1/4} \mathcal{E}_c$ , the superconducting state is destroyed since there is no  $f$  that can satisfy it [1, 4].

The electric field  $\mathcal{E}$  in Eq. (6) is the effective field penetrating the superconductor. Because of screening effects, this could be different from the applied electric field  $\mathcal{E}_{ext}$ . We assume that  $\mathcal{E} = \chi \mathcal{E}_{ext}$  where  $\chi$  is a screening parameter.

It is natural to assume that the screening parameter depends on temperature. At  $T = 0$  we assume no screening, i.e.,  $\chi(T = 0) = 1$  and  $\mathcal{E} = \mathcal{E}_{ext}$ . At the critical temperature, the system becomes normal and, because of almost perfect screening, the electric field does not penetrate the metal; therefore, we have  $\chi(T = T_c) = 1$  and  $\mathcal{E} = 0$  inside the superconductor. With these observations, we assume a temperature dependence of  $\chi$

$$\chi(T) = \left(1 - \frac{T}{T_c}\right)^\eta = \bar{\alpha}^\eta. \quad (7)$$

and we obtain a modified equation for  $f$

$$f^2 = 1 - \frac{1}{\bar{\alpha}^{1-4\eta}} \left(\frac{\mathcal{E}_{ext}}{\mathcal{E}_c}\right)^4. \quad (8)$$

From Eq. (8), we can infer a phenomenological behavior of the critical current. In absence of magnetic and electric field, the critical current reads  $I_c = \frac{8}{3\sqrt{3}} \frac{e}{\sqrt{m}\beta} |\alpha|^{3/2}$  [1, 2]. The information about the superconductivity suppression can be included by modifying the critical current (normalized to  $I_c^0 \equiv I_c(T = 0, \mathcal{E} = 0)$ ) as

$$\begin{aligned} \frac{I_c}{I_c^0} &= \bar{\alpha}^{3/2} \left[1 - \frac{1}{\bar{\alpha}^{1-4\eta}} \left(\frac{\mathcal{E}_{ext}}{\mathcal{E}_c}\right)^4\right]^\gamma \\ &= \left(1 - \frac{T}{T_c}\right)^{3/2} \left[1 - \frac{1}{(1 - T/T_c)^{1-4\eta}} \left(\frac{\mathcal{E}_{ext}}{\mathcal{E}_c}\right)^4\right]^\gamma \end{aligned} \quad (9)$$

where  $\eta$  and  $\gamma$  are parameters to be determined with the experimental data. We can rewrite the critical current expression as a function of a critical voltage  $V_g$  with  $\mathcal{E}_{ext}/\mathcal{E}_c = V_g/V_g^c$ . The plots in Fig. 2c of the main text are obtained for  $\eta = 1/4$  and  $\gamma = 3/2$ .

### Critical current with electric and magnetic field

The description of the critical current behaviour in presence of both electric  $\mathcal{E}$  and magnetic field  $B$  is more complex. It is known that the presence of a magnetic field reduces the critical

current and the standard theory predicts a decrease with  $B$  (see Refs. [1, 2, 4–6]).

However, as shown in Fig. 3a of the main text, the experimental measured values of the critical current at  $\mathcal{E} = 0$  have a complex dependence on  $B$ . In particular the oscillator behavior at high magnetic field, are related to the Weber blockade [7] that is not accounted in the standard theory [1, 4–6]. For this reason, here we adopt a more practical approach.

From the previous discussion we know that the critical current is suppressed as  $(\mathcal{E}_{ext}/\mathcal{E}_c)^4$ . To include the magnetic field dependence, we use the phenomenological function

$$\frac{I_c}{I_c^0} = I_{meas}(B) \left[1 - \left(\frac{\mathcal{E}_{ext}}{\mathcal{E}_c}\right)^4\right]^\gamma = I(B) \left[1 - \left(\frac{V_g}{V_g^c}\right)^4\right]^\gamma \quad (10)$$

where  $I_{meas}(B) \equiv I_{meas}(B, \mathcal{E} = 0)$  is the (normalized) value of the critical current measured at  $B$  and  $\mathcal{E} = 0$ . Since the measurements are done at constant and low temperature ( $T = 10$  mK corresponding to  $T/T_c = 0.03$ ), we can assume  $\bar{\alpha} \approx 1$ . The plots in Fig. 3d of the main text are obtained from Eq. (10) with  $\gamma = 3/2$ .

### Supplementary Information References

\* [francesco.giazotto@sns.it](mailto:francesco.giazotto@sns.it)

- [1] de Gennes, P. G. *Superconductivity of Metals and Alloys*, Advanced Books Classics (Westview Press, 1999).
- [2] Tinkham, M. *Introduction to Superconductivity* (McGraw-Hill, 1996).
- [3] Ginzburg, V. L. & Landau, L. D. On the theory of superconductivity. *Zh. Eksp. Teor. Fiz.* **20**, 35 (1950).
- [4] Schmidt, V., Müller, P & Ustinov, A., *The Physics of Superconductors: Introduction to Fundamentals and Applications* (Springer, 1997)
- [5] Bardeen, J. Critical Fields and Currents in Superconductors. *Rev. Mod. Phys.* **34**, 667 (1962).
- [6] Mydosh, J. A. & Meissner, H. Dependence of the Critical Currents in Superconducting Films on Applied Magnetic Field and Temperature. *Phys. Rev.* **140**, A1568 (1965).
- [7] Morgan-Wall, T., Leith, B., Hartman, N., Rahman, A. & Marković, N. Measurement of Critical Currents of Superconducting Aluminum Nanowires in External Magnetic Fields: Evidence for a Weber Blockade. *Phys. Rev. Lett.* **114**, 077002 (2015).